

Lattice dynamics and elastic properties of the 4*f* electron system: CeNV. Kanchana,¹ G. Vaitheeswaran,² Xinxin Zhang,³ Yanming Ma,³ A. Svane,⁴ and O. Eriksson⁵¹*Department of Physics, Indian Institute of Technology Hyderabad, Ordinance Factory Estate, Yeddumailaram 502 205, Andhra Pradesh, India*²*Advanced Centre of Research in High Energy Materials (ACRHEM), University of Hyderabad, Prof. C. R. Rao Road, Gachibowli, Hyderabad 500 046, Andhra Pradesh, India*³*National Laboratory of Superhard Materials, Jilin University, 130012, Changchun, China*⁴*Department of Physics and Astronomy, Aarhus University, DK-8000 Aarhus C, Denmark*⁵*Department of Physics and Astronomy, Uppsala University, Box 516, SE-751 20, Uppsala, Sweden*

(Received 19 July 2011; published 21 November 2011)

The electronic structure, structural stability, and lattice dynamics of cerium mononitride are investigated using *ab initio* density-functional methods involving an effective potential derived from the generalized gradient approximation and without special treatment for the 4*f* states. The 4*f* states are hence allowed to hop from site to site, without an on-site Hubbard *U*, and contribute to the bonding, in a picture often referred to as *itinerant*. It is argued that this picture is appropriate for CeN at low temperatures, while the anomalous thermal expansion observed at elevated temperatures indicates entropy-driven localization of the Ce *f* electrons, similar to the behavior of elemental cerium. The elastic constants are predicted from the total energy variation of strained crystals and are found to be large, typical for nitrides. The phonon dispersions are calculated showing no soft modes, and the Grüneisen parameter behaves smoothly. The electronic structure is also calculated using the quasiparticle self-consistent GW approximation (where *G* denotes the Green's function and *W* denotes the screened interaction). The Fermi surface of CeN is dominated by large egg-shaped electron sheets centered on the *X* points, which stem from the *p*-*f* mixing around the *X* point. In contrast, assuming localized *f* electrons leads to a semimetallic picture with small band overlaps around *X*.

DOI: [10.1103/PhysRevB.84.205135](https://doi.org/10.1103/PhysRevB.84.205135)

PACS number(s): 71.20.Eh, 63.20.dk, 71.18.+y, 65.40.De

I. INTRODUCTION

CeN is the first member of the series of rare-earth mononitrides,^{1,2} which all crystallize in the rock-salt crystal structure. The rare-earth mononitrides have received renewed attention due to their peculiar electronic and magnetic properties and their potential application in spintronics.^{3–6} CeN is different from the other members of the series in several respects. The lattice constant of CeN is significantly smaller^{1,4} than for the other rare-earth mononitrides, while the susceptibility is characteristic of a temperature-independent paramagnet,^{1,7} in contrast to the local moment magnetism encountered in the later nitrides.⁴ Furthermore, the thermal expansion shows an unusual increase in lattice parameters at elevated temperatures accompanied by a dip in the susceptibility^{7–9} and an increase in resistivity and Seebeck coefficients.¹⁰ Also, a change in reflectivity with temperature has been observed,¹¹ and anomalous lattice expansion upon alloying with O occurs.¹²

All these observations suggest that the rigid trivalent picture of the Ce ions in CeN with localized *f*¹ electrons is inadequate, and instead *f* electrons contribute to the chemical bonding. In the mixed-valent picture,^{13–15} the localized *f* electrons hybridize weakly with the conduction electrons, leading to a ground state composed of a mixture of *f*⁰ and *f*¹ ions. This leads to an effective Ce valence in CeN between 3 and 4, which becomes very sensitive to external parameters like pressure and temperature. Core-level photoemission spectroscopy on CeN show clear signals of both valencies,¹⁶ while the interpretation of absorption spectra is less clear.^{8,17} Valence photoemission experiments^{16,18} as well as inverse photoemission spectra¹⁹ are often interpreted in the Gunnarsson-Schönhammer model²⁰ (GS), which considers a single Ce impurity in a conduction sea. The Ce ion fluctuates between the *f*⁰ and *f*¹ configuration,

which models the mixed-valent state. However, for CeN the energy of the *f*¹ state is much lower than that of the *f*⁰ state, and the GS picture of the ground state becomes that of Kondo screened local moments.¹⁸ The derived Kondo temperature for CeN is in between those of the α and γ phases of elemental Ce (Ref. 18). The effective Ce valence is near to 3 (see Ref. 21). In contrast, optical conductivity data have been interpreted in terms of an effective valence of 3.48,²² while the effective valence extracted from the lattice constant is much closer to 4, around 3.85 at room temperature but approaching 3 at temperatures around 1100 K.⁷ This latter result is in accordance with the Kondo model, where an effective valence around 3 at high temperatures is reached as a result of the destruction of the screening and the formation of disordered local *f* moments.

A picture different from the Kondo screened scenario is offered by the itinerant electronic structure approach,^{23–25} according to which the *f* electrons form coherent band states with a total bandwidth of 2 eV and a high density of states at the Fermi level. This picture makes the assumption that the on-site Coulomb interaction is not dominating the problem and that all correlation effects can be incorporated in the effective potential of the 4*f* states. We refer to this as the “band picture” of the Ce 4*f* states. The occupied *f* states lead to a ~ 0.5 -eV-wide peak in the density of states just below the Fermi level,^{23,24} in good agreement with the valence photoemission experiments.^{16,18} This peak integrates to an *f* occupancy of approximately 1, in good agreement with the nearly trivalent picture offered by the Kondo picture. At the same time, the calculated lattice constant^{24,25} is in good agreement with the experimental value at low temperature, due to the substantial bonding provided by the *f*-band states; that is, the ground

state is not trivalent in the traditional sense with localized corelike f electrons. The inverse photoemission spectrum of CeN (Ref. 19) shows f character just above the Fermi level, which also concurs with the occurrence of a Ce f band pinned to the Fermi level. However, not all measured spectral properties of the unoccupied $4f$ states are reproduced by this picture. In particular, the distinct feature observed¹⁹ at 6 eV above the Fermi energy cannot be explained but rather reflects the large on-site Coulomb correlation energy associated with the formation of f^2 ions in the inverse photoemission process. The optical conductivity calculated in the band picture is in excellent agreement with experimental data, in contrast to the result based on a localized (corelike) picture of f electrons.²⁵ Also, the magnetic susceptibility and linear specific heat coefficient calculated assuming f -band formation compares favorably with the experimental data.²⁵ In particular, the latter comes out too high in the Kondo picture.¹⁸

The systematics of the Ce pnictides have been investigated in experiment^{16,26} and theory,²⁷ showing the peculiar role of CeN. The heavier pnictides display pure trivalent core-level photoemission spectra but exhibit valence transitions induced by pressure, whereas CeN appears to be on the other side of the valence transition already at ambient pressure. The self-interaction corrected (SIC) local spin density (LSD) calculations of Refs. 27 and 28 find a near degeneracy of the localized f^1 and bandlike scenarios for CeN but clear preference for the localized scenario for the later pnictides.

In the present paper, further investigations of CeN are undertaken, implementing both the band picture and the localized picture of the f electrons. Specifically, the elastic constants, pressure-volume curve, Fermi surface, and lattice dynamics are discussed. The results point toward the band picture being most appropriate for CeN at low temperature, while the unusual thermal expansion data measured at elevated temperatures may be due to a temperature-driven transition into a trivalent state of the Ce ions, similar to the $\alpha \rightarrow \gamma$ transition seen in elemental cerium.²⁹ The paper is organized in the following way: Sec. II discusses the methodology and the details of the computations. Ground-state properties, elastic constants, and phonon dispersions are presented in Sec. III, and the electronic structure is discussed in Sec. IV. Finally, Sec. V concludes the paper.

II. COMPUTATIONAL DETAILS

A series of theoretical tools have been employed to study the electronic structure of CeN. The all-electron full potential (FP) linear muffin-tin orbital method³⁰ (LMTO) is used to calculate the total energies as well as the ground-state properties.³¹ Here the crystal is divided into two regions: nonoverlapping muffin-tin spheres surrounding each atom and the interstitial region between the spheres. We used a double- κ $spdf$ LMTO basis (each radial function within the spheres is matched to a Hankel function in the interstitial region of decay constant κ) for describing the valence bands. Basis functions of Ce($5s, 6s, 5p, 5d, 4f$) and N($2s, 2p$) character have been used in the calculation. Within the spheres, the potential is expanded in terms of spherical harmonics, while in the interstitial region it is expanded in terms of plane waves. Both the local density approximation³² (LDA) and

the generalized gradient approximation³³ (GGA) have been used for the exchange-correlation potential. In both cases, the f electrons move in the effective potential generated by the total density and are allowed to hybridize and form bands; that is, these approaches include a band formation energy contribution from the f electrons. This may equally well be interpreted as the density-functional representation of the Kondo screening energy. The charge density and potential inside the muffin-tin spheres were represented by spherical harmonics up to $l_{\max} = 6$, while in the interstitial region, 6566 plane waves with the energies up to 147.5 Ry were included in the calculations. Total energies were evaluated as functions of volume with the tetrahedron method for a $22 \times 22 \times 22$ k mesh, which corresponds to 328 k points in the irreducible Brillouin zone, and were fitted to the Birch equation of state³⁴ to obtain the basic ground-state properties. The elastic constants were obtained from the variation of the total energy with volume-conserving strains, as outlined in Ref. 35.

The electronic structure and Fermi surface of CeN has been calculated with the quasiparticle self-consistent GW (where G denotes the Green's function and W denotes the screened interaction) approximation³⁶ (QSGW), in the FP-LMTO implementation of Ref. 37. This calculation also included a double- κ LMTO basis set. For an accurate description of the polarization function, the basis set was augmented with high-lying N $3s$ and $3p$ as well as interstitial "floating" orbitals.³⁷ Furthermore, inside muffin-tin spheres a product basis set was used.³⁸ An $8 \times 8 \times 8$ Monkhorst-Pack (MP) k mesh was used for the calculation of the screened interaction, which is evaluated in the random-phase approximation. The special feature of the quasiparticle self-consistency is that the one-particle band structure, which is used as input for the evaluation of the GW eigenenergies, is iterated so as to come as close as possible to the output band GW structure.³⁶

The calculation of the phonon frequencies of CeN were based on the density-functional linear-response approach³⁹ in the GGA³³ combined with the plane-wave pseudopotential method as implemented in the PWSCF package.⁴⁰ Ultrasoft Vanderbilt pseudopotentials were used with the valence configurations of $4f^1 5s^2 5p^6 5d^1 6s^2$ for Ce and $2s^2 2p^3$ for N. The Brillouin-zone integrations were carried out with a $10 \times 10 \times 10$ MP k grid and a kinetic energy cutoff of 60 Ry was used. A $4 \times 4 \times 4$ mesh in the first Brillouin zone was used in the interpolation of the force constants for the phonon dispersion curve calculations. The theoretical equilibrium lattice constant of 5.05 Å, which is slightly larger than the experimental data 5.04 Å, was used in the phonon dispersion calculations.

The localized f -electron picture is suitably implemented with the self-interaction corrected local spin density (SIC-LSD) approximation.⁴¹ The tight-binding LMTO method⁴² was employed in the calculations, and a single localized f electron on each Ce atom has been assumed, while other electronic degrees of freedom have been described as Bloch states. A single $spdf$ basis set was used in this case, with a $16 \times 16 \times 16$ k mesh. These calculations are similar to those reported in Refs. 27 and 28. The spin-orbit interaction is included in the Hamiltonian. The total energy of the state with localized f electrons is compared to the energy of the

scenario where all f electrons are treated as band states. The self-interaction correction represents an energy gained by localization, which competes with the band formation energy for itinerant states. For the later Ce mononitrides, CeAs, CeSb, and CeBi, the localized picture is energetically advantageous; however, for CeN the itinerant treatment of f electrons gives a marginally lower energy.^{27,28}

III. GROUND-STATE AND ELASTIC PROPERTIES

The calculated ground-state properties, equilibrium lattice constant, and bulk modulus and its pressure derivative are given in Table I along with earlier experimental and theoretical results. The calculated bulk modulus of 158 GPa in GGA is in excellent agreement with the experimental value of 153 GPa.⁴³ The experimental lattice constant of CeN is 5.01 Å, which is substantially lower than the value ~ 5.2 Å obtained by extrapolation of the lattice constant of the later rare-earth nitrides^{3,4} and indicates that the Ce ions in CeN are not purely trivalent, as opposed to the later rare-earth ions in their mononitrides. On the other hand, the value of $a \sim 5.19$ Å is reached by experiment at very high temperatures, $T \sim 1100$ K, following the unusual thermal expansion in the temperature range from 400 to 1100 K.⁹ The lattice constant obtained in the present theory using the GGA is slightly above the experimental value, while the LDA value is significantly below, features which are common for these approaches. Therefore, the band picture anticipated in the GGA appears to be well suited for calculations of the equilibrium properties of CeN at low temperatures. In the localized picture, implemented in SIC-LSD, the state exhibiting localized f^1 Ce ions is found to be energetically less favorable than the itinerant state,²⁷ albeit with a small difference in total energy, which in the present work is calculated as 0.2 eV per CeN formula

TABLE I. Ground-state properties, lattice constant a (in Å), bulk modulus B_0 (in GPa), and pressure derivative of the bulk modulus, B'_0 , for CeN at ambient pressure, as calculated in the present work using the LDA, the GGA, and the SIC-LSD approaches. Sources of experimental data are indicated in the notes. The last line gives the lattice constant and bulk modulus for LaN for comparison.

	a (Å)	B_0 (GPa)	B'_0
LDA	4.94	181.1	3.6
GGA	5.02	158.1	3.3
SIC Ce(f^1)	5.14	141.0	3.1
Expt.	5.007 ^a	153, ^b 92 ^c	
Other theory	4.87, ^d 4.97, ^e 5.04, ^f 5.35 ^g	159 ^d	
LaN	5.21, ^h 5.30, ⁱ 5.39 ^g , 5.16 ^j	149.2, ^h 131.1, ⁱ 152 ^{g,j}	

^aRef. 10.

^bRef. 43.

^cExtracted from data published in Ref. 7.

^dTB-LMTO results of Ref. 27.

^eFP-LMTO, Ref. 25, LDA.

^fAs e, but GGA.

^gHartree-Fock calculations of Ref. 44.

^hPresent work, LDA.

ⁱPresent work, GGA.

^jRef. 45, LDA.

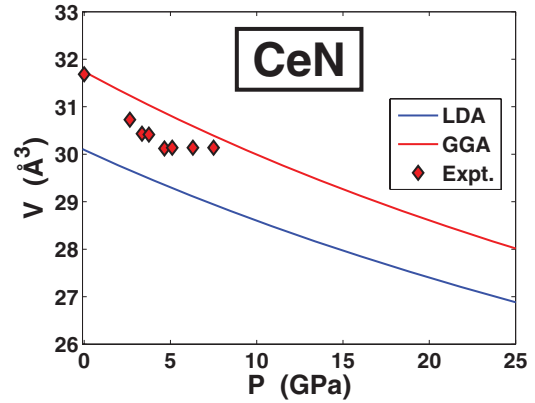


FIG. 1. (Color online) Calculated pressure-volume relation of CeN using the LDA and GGA exchange-correlation functionals. The points marked are the experimental data from Ref. 7.

unit. The SIC-LSD theory pertains only to zero temperature; however, one may speculate that entropic effects will become significant enough to overcome this energy barrier at high temperatures, causing a localization transition.²⁷ The entropy of a localized f^1 ion is presumably of order $\Delta S \sim k_B \log 6$, due to the degeneracy of the $j = \frac{1}{2}$ level, which then leads to an order-of-magnitude estimate of the transition temperature of $T \sim \Delta E / \Delta S \sim 1300$ K, in good agreement with the experimental anomalies occurring in the range 400–1000 K. The lattice constant of the localized state, as calculated with SIC-LSD, is found to be $a = 5.14$ Å, also fairly close to the high-temperature limit.

The pressure-volume relation, as calculated within the LDA and GGA for the exchange-correlation potential, is shown in Fig. 1. The pressure-volume curve is smooth, while the few experimental data points from Ref. 7 show a somewhat unusual behavior, with first a swift decrease in lattice constant followed by a range $4 \text{ GPa} < p < 8 \text{ GPa}$ in which the lattice constant does not change. Similar behavior was found in LaN, NdN, and ErN, although with a somewhat smaller initial softening, which was interpreted by Olcese in Ref. 7 as a signature of an increasing effective valence of Ce in CeN as pressure is increased. The observation of a pressure range with zero compressibility for all four rare-earth mononitrides is suspicious, though, and more experimental investigations are needed. The bulk modulus extracted by the present authors from the data of Ref. 7, $B_0 = 92$ GPa, is significantly below the value reported in Ref. 43, $B_0 = 153$ GPa.

The calculated elastic constants and the other mechanical properties derived from these are collected in Table II. They are all positive, as they must be for a mechanically stable crystal structure. The elastic constants still await experimental confirmation, which would be an important contribution to the discussion of the electronic structure of CeN, in particular since a negative C_{12} sometimes serves as a fingerprint of mixed valent behavior.^{14,46} The Young's modulus has been estimated from experiments on thin films of CeN grown on a MgO substrate to be $E = 330(16)$ GPa,⁴⁷ which is almost 50% larger than the values calculated by LDA and GGA in Table II.

For comparison, the calculated properties of LaN have also been included in Table I. Often lanthanum compounds may be regarded as non- f materials with equivalent properties to their

TABLE II. The calculated elastic constants C_{ij} , Young's modulus E , shear modulus G , Poisson's ratio σ , B/G ratio, and Debye temperature θ_D of CeN.

	Unit	LDA	GGA
C_{11}	GPa	328.8	310.2
C_{12}	GPa	70.0	83.2
C_{44}	GPa	60.8	72.6
E	GPa	227.7	224.8
G	GPa	88.2	88.9
σ		0.291	0.264
B/G		2.05	1.79
θ_D	K	433.4	437.3

later rare-earth homologues; for example, for LaSb and CeSb, identical compression curves have been measured.⁴⁸ For LaN this is not quite the case, as the calculated bulk modulus is in fact smaller for LaN than for CeN, in both LDA and GGA, the reason being that the Ce f electrons are not localized and nonbonding in these calculations.

According to Pugh,⁴⁹ the ratio of bulk to shear modulus, B/G , may be used to determine whether a compound be brittle ($B/G < 1.75$) or ductile ($B/G > 1.75$). For CeN, we obtain the value $B/G = 1.79$, slightly to the ductile side. Frantsevich,⁵⁰ on the other hand, suggested using the Poisson ratio for this distinction, classifying compounds with $\sigma < \frac{1}{3}$ as brittle, and those with $\sigma > \frac{1}{3}$ as ductile. In the present case, we find $\sigma = 0.264$, well on the brittle side, which is contradictory to the Pugh criterion but illustrates the uncertainty of the concept. A similar situation has been observed in Fe_2VGa (Ref. 51) and MgCNi_3 (Ref. 52). The nature of the bonding can also be revealed from the Cauchy's pressure, which is given by $C_p = C_{12} - C_{44} = 10$ GPa for CeN. According to Pettifor,⁵³ this positive value of C_p relates to a more ionic character of the bonding in CeN.

The calculated phonon dispersion curves and the corresponding phonon density of states are shown in Fig. 2. There are no imaginary phonon frequencies in the entire Brillouin zone, which shows the dynamical stability of CeN at ambient condition within the GGA. From the projected phonon density

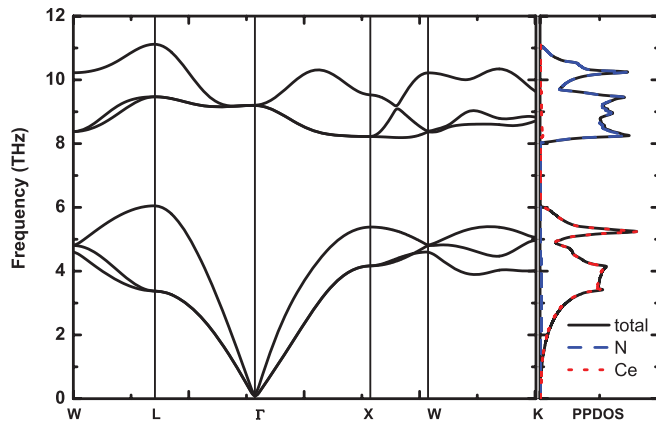


FIG. 2. (Color online) Calculated phonon dispersion relation of CeN. The panel to the right illustrates the atom-projected phonon density of states.

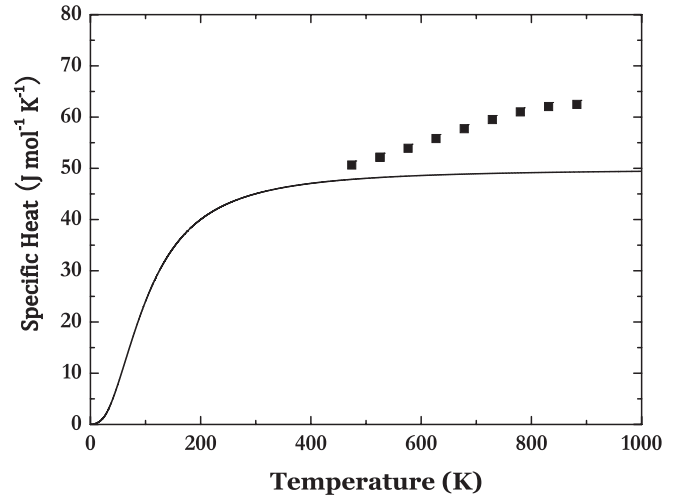


FIG. 3. Calculated specific heat of CeN, compared to the experiment of Ref. 9.

states in Fig. 2, one can see that Ce atoms mainly contribute to the low-frequency vibrations, while N atoms dominate the high-frequency vibrations, which merely reflect the ratio of the masses of the constituent atoms.

Within the quasiharmonic approximation, the phonon contribution to the total specific heat of the crystal may be expressed as a sum over all modes in the Brillouin zone (BZ):⁵⁴

$$C_v(T) = \sum_{\mathbf{q},j} C_{v,j}(\mathbf{q},T), \quad (1)$$

where the individual mode contribution is given by

$$C_{v,j}(\mathbf{q},T) = \frac{\hbar\omega_j(\mathbf{q},V)}{V} \frac{d}{dT} \left[\exp\left(\frac{\hbar\omega_j(\mathbf{q},V)}{k_B T}\right) - 1 \right]^{-1}. \quad (2)$$

Here, $\omega_j(\mathbf{q},V)$ is the phonon frequency of the j th mode at wave vector \mathbf{q} in the BZ. The calculated phonon part of the specific heat of CeN is shown in Fig. 3. The standard Debye shape is found, which approaches the Dulong-Petit limit $C_v \sim 6R = 50$ J/(mol K) from temperatures $T \sim 500$ K and above. In contrast, the experimental data points⁹ are higher than the calculated harmonic C_v , increasing toward 62 J/(mol K) at $T \sim 900$ K, which shows that additional entropy is stored in the system. This could be due to anharmonic effects, possibly combined with the formation of disordered local moments.

The Grüneisen parameter $\gamma_j(\mathbf{q})$ corresponding to the (\mathbf{q},j) phonon mode is defined as⁵⁴

$$\gamma_j(\mathbf{q}) = -\frac{\partial \ln \omega_j(\mathbf{q})}{\partial \ln V}, \quad (3)$$

and the overall Grüneisen parameter is given as the weighted average of the mode Grüneisen parameters:

$$\gamma(T) = \frac{\sum_{\mathbf{q},j} \gamma_j(\mathbf{q}) C_{v,j}(\mathbf{q},T)}{C_v(T)}. \quad (4)$$

The calculated Grüneisen parameter of CeN is shown in Fig. 4. The Grüneisen parameter is seen to increase with temperature and saturate at a value around 1.8 at large temperatures ($T \sim 800$ K). A high temperature value of the thermal expansion

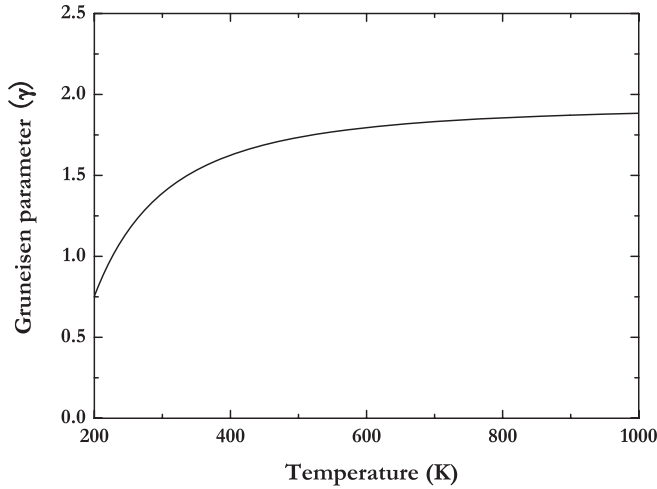


FIG. 4. Calculated Grüneisen parameter of CeN, see Eq. (4).

may be obtained by using this value in the simple expression for the linear thermal expansion coefficient, α :⁵⁴

$$\alpha = \frac{\gamma C_v}{3B_0}, \quad (5)$$

which leads to $\alpha \simeq 10^{-5} \text{ K}^{-1}$ using the Dulong-Petit limit for C_v and the calculated bulk modulus (cf. Table I). The thermal expansion coefficient was measured by Ref. 9 and exhibits an unusual behavior. In the temperature range $200 \text{ K} < T < 1000 \text{ K}$, the expansion rises from a level around $\alpha \simeq 10^{-5} \text{ K}^{-1}$ in a broad bell-shaped fashion to reach a maximum of $\alpha \simeq 4.5 \times 10^{-5} \text{ K}^{-1}$ around 700 K. Scram *et al.* (Ref. 9) further showed that the anomalous behaviors of the thermal expansion and the specific heat are consistent if a value of $\gamma = 2.1$ is assumed for the Grüneisen parameter, which is not far from our high temperature limit ($\gamma = 1.8$) in Fig. 4. Unfortunately, the experiments shed no light on the origin of the anomaly, one possibility being the onset of localization of the Ce f electrons.

IV. ELECTRONIC STRUCTURE

In Fig. 5, the electronic structure of CeN as calculated using the LDA [Fig. 5(a)], the QSGW approximation [Fig. 5(b)], and the SIC-LDA approach [Fig. 5(c)] with one localized f electron are shown. With one localized f electron, Ce is formally in a trivalent state, which matches the pentavalence of N. Therefore, the N p bands are essentially filled, and the SIC-LSD band picture in Fig. 5(c) becomes semimetallic, with the N p bands forming the valence bands from -4 eV to 0 , where 0 marks the Fermi energy. A small band overlap occurs at X, leading to the semimetallic nature. This conforms with the generic picture of most rare-earth mononitrides, which exhibit small indirect band gaps $\Gamma - X$ and small direct gaps at X, which in some cases may close.^{3,5} In contrast, in the itinerant picture of the LDA in Fig. 5(a), Ce is in a tetravalent state, and one more electron state must be occupied, which leads to a metallic picture with the Fermi level occurring at the bottom of the f bands. In the QSGW band structure in Fig. 5(b), the same metallic picture emerges. The ensuing Fermi surface, Fig. 6, is characterized by large egg-shaped electron pockets around the X points, which originate from

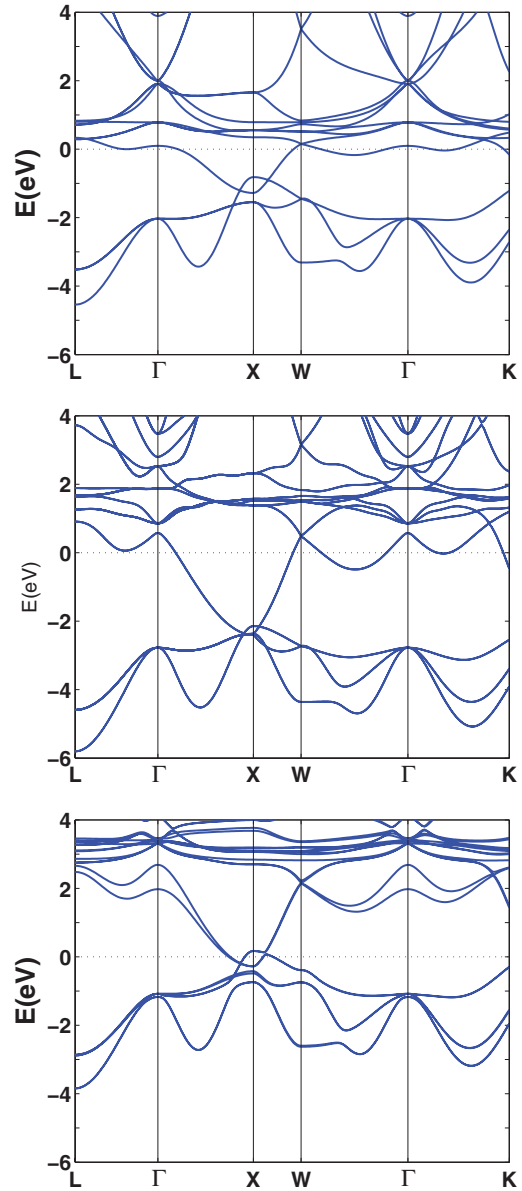


FIG. 5. (Color online) Electronic structure of CeN as calculated (a): in the LDA, (b): in the QSGW approximation, and (c): in the SIC-LDA with one localized f -electron; only the itinerant states are shown.

the strongly p - f hybridized band, which dips down from the f -band manifold at the X points in Figs. 5(a) and 5(b). The QSGW increases the separation of the valence N p bands from the Ce f bands; that is, the f bands shift up by $\sim 1 \text{ eV}$ and the N p bands shift down by $\sim 1 \text{ eV}$ relative to the Fermi level in QSGW compared to LDA. However, the crossings of bands with the Fermi level are very nearly the same in LDA and QSGW, so the Fermi surfaces are similar. In contrast, the SIC-LSD Fermi surface (not shown), due to the semimetallic band structure in Fig. 5(c), consists of small electron and hole pockets around X. Hence, an experimental determination of the Fermi surface of CeN should be a strong tool for experimental clarification of the state of the Ce f electrons in this compound. Another significant feature of the band structures in Fig. 5 is the different positions of the f bands

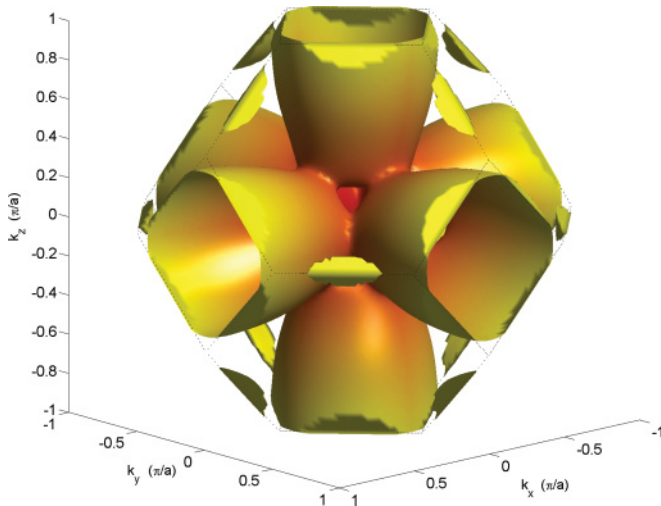


FIG. 6. (Color online) Fermi surface of CeN as calculated in the QSGW approximation. The dashed lines mark the fcc Brillouin zone edges. The coloring is only for presentation purposes.

(0.6, 1.6, and 3.4 eV above the Fermi level for the LDA, QSGW and SIC-LSD approaches, respectively). Neither of these describe fully the ~ 6 -eV feature observed in inverse photoemission experiments.¹⁹ Similarly, the N p -band positions are markedly different; for example, the triply degenerate N p -band state at Γ is situated at approximately -2.0 , -2.8 , and -1.1 eV relative to the Fermi level in LDA, QSGW and SIC-LSD, respectively. The QSGW furthermore enhances the width of the N p band by ~ 0.6 eV.

V. CONCLUSIONS

The ground-state properties and electronic structure of CeN have been investigated by several theoretical tools. The results

have been discussed in relation to available experimental information and with emphasis on the nature of the Ce f states in this compound. The lattice constant and bulk modulus are calculated with the generalized gradient approximation for the total energy, which includes a cohesive contribution due to the f electrons, and agree well with available experimental information. The elastic constants and phonon dispersion relations obtained using the GGA, as well as the Fermi surface, are other fundamental properties by which future experimental determinations may assist in clarifying the role of the f states in this compound. The unusual experimental results for the specific heat and lattice expansion at elevated temperatures suggest that a localization transition occurs in CeN with temperature, similar to the $\alpha \rightarrow \gamma$ transition observed for elemental cerium. This is consistent with the Kondo picture of CeN, where the screening of Ce f moments is destroyed by increased temperatures, leading to fluctuating local moments. In the density-functional framework, this may be the state represented in the SIC-LSD approximation with one localized (corelike) f state per Ce atom, in which case virtually no cohesive energy is associated with the f electrons.

ACKNOWLEDGMENTS

O.E. acknowledges support from the Swedish Research Council, KAW Foundation, STEM, and ERC (Grant No. 247062-ASD). Part of the calculations were carried out at the Center for Scientific Computing in Aarhus (CSCAA) supported by the Danish Center for Scientific Computing. Y.M. acknowledges support from the National Natural Science Foundation of China (under Grants No. 11025418 and No. 91022029).

¹R. Didchenko and F. P. Gortsema, *J. Phys. Chem. Solids* **24**, 863 (1963).

²F. Hulliger, in *Handbook on the Physics and Chemistry of Rare Earths*, edited by K. A. Gschneidner Jr. and L. Eyring (North-Holland, New York, 1979), Vol. 4, Chap. 33.

³C. M. Aerts, P. Strange, M. Horne, W. M. Temmerman, Z. Szotek, and A. Svane, *Phys. Rev. B* **69**, 045115 (2004).

⁴C.-G. Duan, R. F. Sabirianov, W. N. Mei, P. A. Dowben, S. S. Jaswal, and E. Y. Tsymlal, *J. Phys. Condens. Matter* **19**, 315220 (2007).

⁵P. Larson, W. R. L. Lambrecht, A. Chantis, and M. van Schilfgaarde, *Phys. Rev. B* **75**, 045114 (2007).

⁶A. R. H. Preston, S. Granville, D. H. Housden, B. Ludbrook, B. J. Ruck, H. J. Trodahl, A. Bittar, G. V. M. Williams, J. E. Downes, A. DeMasi, Y. Zhang, K. E. Smith, and W. R. L. Lambrecht, *Phys. Rev. B* **76**, 245120 (2007).

⁷G. L. Olcese, *J. Phys. F* **9**, 569 (1979).

⁸J. P. Kappler, E. Beaupaire, G. Krill, J. Serenis, C. Godrat, and G. Olcese, *J. Phys. I* **1**, 1381 (1991).

⁹R. P. C. Schram, J. G. Boshoven, E. H. P. Cordfunke, R. J. M. Konings, and R. R. van der Laan, *J. Alloys Compd.* **252**, 20 (1997).

¹⁰J. Danan, C. de Novion, and R. Lallemand, *Solid State Commun.* **7**, 1103 (1969).

¹¹J. Schlegel, E. Kaldis, P. Wachter, and C. Zürcher, *Phys. Lett. A* **66**, 125 (1978).

¹²R. C. Brown and N. C. Clark, *J. Inorg. Nucl. Chem.* **36**, 1777 (1974).

¹³C. M. Varma, *Rev. Mod. Phys.* **48**, 219 (1976).

¹⁴P. Wachter, in *Handbook on the Physics and Chemistry of Rare Earths*, edited by K. A. Gschneidner Jr., L. Eyring, G. H. Lander, and G. R. Choppin (North-Holland, Amsterdam, 1994), Vol. 19, Chap. 132.

¹⁵A. Jayaraman, in *Handbook on the Physics and Chemistry of Rare Earths*, edited by K. A. Gschneidner Jr. and L. Eyring (North-Holland, New York, 1979), Vol. 2, Chap. 20.

¹⁶Y. Baer and Ch. Zürcher, *Phys. Rev. Lett.* **39**, 956 (1977); Y. Baer, R. Hauger, Ch. Zürcher, M. Campagna, and G. K. Wertheim, *Phys. Rev. B* **18**, 4433 (1978).

- ¹⁷D. Malterre, C. Brouder, G. Krill, E. Beaurepaire, B. Carrière, and D. Chandesris, *Europhys. Lett.* **15**, 687 (1991).
- ¹⁸F. Patthey, S. Cattarinussi, W.-D. Schneider, and Y. Baer, *Europhys. Lett.* **2**, 883 (1986); F. Patthey, J.-M. Imer, W.-D. Schneider, H. Beck, Y. Baer, and B. Delley, *Phys. Rev. B* **42**, 8864 (1990).
- ¹⁹E. Wuilloud, B. Delley, W.-D. Schneider, and Y. Baer, *J. Magn. Magn. Mater.* **47-48**, 197 (1985).
- ²⁰O. Gunnarsson and K. Schönhammer, *Phys. Rev. Lett.* **50**, 604 (1983); *Phys. Rev. B* **28**, 4315 (1983).
- ²¹Reference 18 quotes both values of $n_f = 0.82$ (text) and $n_f = 0.92$ (table and figure) for the f count in their Kondo model calculations for CeN, corresponding to effective valencies of 3.18 or 3.08. Reference 19 gives a value of $n_f = 0.83$ (figure).
- ²²J. Schoenes, in *Handbook on the Physics and Chemistry of the Actinides*, edited by A. J. Freeman and G. H. Lander (North-Holland, Amsterdam, 1984), Vol. 1, Chap. 5; J. Schoenes, in *Moment Formation in Solids*. Proceedings of the NATO Advanced Study Institute, edited by W. J. L. Buyers (Plenum, New York, 1984), p. 237.
- ²³W. E. Pickett and B. M. Klein, *J. Less-Common Met.* **93**, 219 (1983).
- ²⁴M. S. S. Brooks, *J. Magn. Magn. Mater.* **47-48**, 260 (1985).
- ²⁵A. Delin, P. M. Oppeneer, M. S. S. Brooks, T. Kraft, J. M. Wills, B. Johansson, and O. Eriksson, *Phys. Rev. B* **55**, R10173 (1997).
- ²⁶J. M. Léger, *Physics B* **190**, 84 (1993).
- ²⁷A. Svane, Z. Szotek, W. M. Temmerman, and H. Winter, *Solid State Commun.* **102**, 473 (1997); A. Svane, Z. Szotek, W. M. Temmerman, J. Lægsgaard, and H. Winter, *J. Phys. Condens. Matter* **10**, 5309 (1998).
- ²⁸L. Petit, R. Tyer, Z. Szotek, W. M. Temmerman, and A. Svane, *New J. Phys.* **12**, 113041 (2010).
- ²⁹D. C. Koskenmaki and K. A. Gschneidner Jr., in *Handbook on the Physics and Chemistry of Rare Earths*, edited by K. A. Gschneidner Jr. and L. Eyring (North-Holland, New York, 1979), Vol. 1, Chap. 4.
- ³⁰O. K. Andersen, *Phys. Rev. B* **12**, 3060 (1975).
- ³¹S. Y. Savrasov, *Phys. Rev. B* **54**, 16470 (1996).
- ³²S. H. Vosko, L. Wilk, and M. Nusair, *Can. J. Phys.* **58**, 1200 (1980).
- ³³J. P. Perdew, K. Burke, and M. Ernzerhof, *Phys. Rev. Lett.* **77**, 3865 (1996).
- ³⁴F. Birch, *J. Appl. Phys.* **9**, 279 (1938).
- ³⁵V. Kanchana, G. Vaitheeswaran, A. Svane, and A. Delin, *J. Phys. Condens. Matter* **18**, 9615 (2006); V. Kanchana, G. Vaitheeswaran, and A. Svane, *J. Alloys Compd.* **455**, 480 (2008).
- ³⁶T. Kotani, M. van Schilfgaarde, and S. V. Faleev, *Phys. Rev. B* **76**, 165106 (2007).
- ³⁷M. Methfessel, M. van Schilfgaarde, and R. A. Casali, in *Lecture Notes in Physics*, edited by H. Dreyse (Springer-Verlag, Berlin, 2000), Vol. 535, p. 114.
- ³⁸F. Aryasetiawan and O. Gunnarsson, *Phys. Rev. B* **49**, 16214 (1994).
- ³⁹P. Giannozzi, S. de Gironcoli, P. Pavone, and S. Baroni, *Phys. Rev. B* **43**, 7231 (1991).
- ⁴⁰S. Baroni, A. Dalcorso, S. De Gironcoli, P. Giannozzi, C. Cavazzoni, G. Ballabio, S. Scandolo, G. Chiarotti, P. Focher, A. Pasquarello, K. Laasonen, A. Trave, R. Car, N. Marzari, and A. Kokalj, [<http://www.pwscf.org/>].
- ⁴¹A. Svane, *Phys. Rev. B* **53**, 4275 (1996).
- ⁴²O. K. Andersen and O. Jepsen, *Phys. Rev. Lett.* **53**, 2571 (1984).
- ⁴³J. M. Jakobsen, G. K. H. Madsen, J.-E. Jørgensen, J. Staun Olsen, and L. Gerward, *Solid State Commun.* **121**, 447 (2002).
- ⁴⁴E. Voloshina and B. Paulus, *J. Comput. Chem.* **29**, 2107 (2008).
- ⁴⁵G. Vaitheeswaran, V. Kanchana, and M. Rajagopalan, *Solid State Commun.* **124**, 97 (2002).
- ⁴⁶H. Boppart, A. Treindl, P. Wachter, and S. Roth, *Solid State Commun.* **35**, 483 (1980).
- ⁴⁷T.-Y. Lee, D. Gall, C.-S. Shin, N. Hellgren, I. Petrov, and J. E. Greene, *J. Appl. Phys.* **94**, 921 (2003).
- ⁴⁸J. M. Léger, D. Ravot, and J. Rossat-Mignod, *J. Phys. C: Solid State Phys.* **17**, 4935 (1984).
- ⁴⁹S. F. Pugh, *Philos. Mag.* **45**, 823 (1954).
- ⁵⁰I. N. Frantsevich, F. F. Voronov, and S. A. Bokuta, *Elastic Constants and Elastic Moduli of Metals and Insulators Handbook*, edited by I. N. Frantsevich (Kiev, Naukova Dumka, 1983), p. 60.
- ⁵¹V. Kanchana, G. Vaitheeswaran, Y. Ma, Y. Xie, A. Svane, and O. Eriksson, *Phys. Rev. B* **80**, 125108 (2009).
- ⁵²G. Vaitheeswaran, V. Kanchana, A. Svane, and A. Delin, *J. Phys. Condens. Matter* **19**, 326214 (2007).
- ⁵³D. G. Pettifor, *Mater. Sci. Technol.* **8**, 345 (1992).
- ⁵⁴N. W. Ashcroft and N. D. Mermin, *Solid State Physics* (Holt, Rinehart and Winston, New York, 1976).